An Adaptive Regularized Solution to Inverse Ill-Posed Models

Kunpu Ji, Yunzhong Shen, Qiujie Chen, Bofeng Li, and Wei Wang

***Abstract*— The ill-posed models are widely encountered in various inversions of geodesy and remote sensing. The regularization approaches can significantly stabilize the solution to ill-posed models since the high-frequency noise is effectively suppressed. Although the famous Tikhonov regularization and truncated singular value decomposition (TSVD) regularization have been widely applied in various geodetic applications, there still remain theoretical drawbacks for either single regularization. For Tikhonov regularization, given a regularization parameter, the low-frequency terms are over-regularized, and high-frequency terms are under-regularized. For TSVD regularization, some medium-frequency terms will be mistaken for high-frequency terms to be truncated and the hidden signals will be lost. For this reason, we propose an adaptive regularized solution in spectral form, which adaptively divides the terms of different frequencies into three kinds: 1) the low-frequency terms are not regularized; 2) the medium-frequency terms are regularized by the Tikhonov method; and 3) the high-frequency terms are regularized by the TSVD method. The analytical conditions for determining the term sets are derived based on the criteria that the introduced biases should be smaller than the reduced errors; in other words, the mean square error (MSE) should be reduced. The two examples are presented to demonstrate the performance of our adaptive regularization. The first numerical example is solving the Fredholm integral equation of the first kind, which is widely encountered in remote sensing inversions. The simulations clearly demonstrate that the adaptive regularized solution can improve the MSE of ordinary Tikhonov and TSVD regularized functions by 25.00% and 9.09%, respectively. In the second example, we apply the new method to investigate the mass variation of the Yangtze River Basin based on the Gravity Recovery and Climate Experiment (GRACE) time-variable gravity field model. The Tongji-Grace 2018 monthly gravity field solutions from April 2002 to December 2016 are used to construct the mascon observation equation. The results show that our method also outperforms the ordinary Tikhonov and TSVD regularized solutions, with mean MSE reductions of about 13.40% and 11.69%, respectively. Furthermore, the spatial resolution of secular trend derived by our method is improved and the signal-to-noise ratio (SNR) of mass variation series is higher than the other two regularizations.**

***Index Terms*— Ill-posed models, inversion of geodesy and remote sensing, regularized solution, singular value decomposition.**

Manuscript received 17 January 2022; revised 8 May 2022 and 21 July 2022; accepted 17 August 2022. Date of publication 12 September 2022; date of current version 27 September 2022. This work was supported by the Natural Science Foundation of China under Grant 41974002 and Grant 42192532. *(Corresponding author: Yunzhong Shen.)*

The authors are with the College of Surveying and Geo-Informatics, Tongji University, Shanghai 200092, China (e-mail: kunpuji@tongji.edu.cn; yzshen@tongji.edu.cn; chenqiujie2009@163.com; bofeng_li@tongji.edu.cn; wangwei_96@tongji.edu.cn).

This article has supplementary downloadable material available at https://doi.org/10.1109/TGRS.2022.3205572, provided by the authors.

Digital Object Identifier 10.1109/TGRS.2022.3205572

I. Introduction

An ILL-POSED model violates any of the three conditions, i.e., the solution is existent, unique, and stable [1]. For an ill-conditioned linear observational equation, the design matrix is with full-rank, but its singular values decay to zero, and the ratio of the largest over the smallest singular values is significantly amplified; as a result, the very small observation errors will corrupt the resolved parameters considerably. In other words, the solution of an ill-conditioned observational equation is existent and unique but not stable. Such ill-conditioned observational equations are usually discretely formulated and widely encountered in geodesy and remote sensing, such as global navigation satellite system (GNSS) fast ambiguity resolution [2], [3], [4], 3-D GNSS ionospheric tomography [5], [6], gravity field determination from the satellite missions of Gravity Recovery and Climate Experiment (GRACE) [7], [8], [9], [10], [11], [12], [13] or Gravity field and steady-state Ocean Circulation Explorer (GOCE) [14], [15], geometric correction of satellite imagery based on rational function model (RFM) [16], [17], [18], retrieval of vegetation parameters based on radiative transfer model (RTM) [19], [20], and phase unwrapping in synthetic aperture radar interferometry (InSAR) [21], [22].

In order to stabilize the solution, Tikhonov [23], [24] proposed the regularization method, which has been successfully used to solve the inverse ill-posed models. The same mathematical expression with Tikhonov regularization called the ridge regression method was developed by Hoerl and Kennard [25], [26]. Tikhonov regularization is based on the criterion that the two-norm combination of the residuals and parameters is minimized, and the combination parameter is called the regularization parameter. The determination of the regularization parameter is one of the key issues, and once the regularization parameter is fixed, the solution of an ill-posed model is uniquely determined. From the frequentist's point of view, the regularization parameter reduces the impact of observation error on the covariance of estimated parameters, especially for the high-frequency terms with small singular values, but it will introduce biases to the estimated parameters. Therefore, minimizing the mean square error (MSE) of a regularized solution is a reasonable criterion to determine the best regularization parameter [26], [27], [28]. In addition, the regularization parameter can also be determined by the generalized cross-validation (GCV) method [29], L-curve method [30], and variance component estimation method [31]. Since the high-frequency components with small singular values are unreliable, one can also directly truncate the small

singular values that convert the ill-conditioned design matrix to a rank-deficient matrix and then performs pseudoinversion to derive a stable solution, which is referred to as truncated singular value decomposition (TSVD) regularization [32], [33]. Therefore, the number of small singular values to be truncated plays a key role in the TSVD method, which can also be determined by using the abovementioned criteria. Xu [33] pointed out that the L-curve method is usually over-regularized and the MSE method can derive better results. We may like to note that though Tikhonov and TSVD regularizations have been widely used to solve the inverse ill-posed models, there exist other types of regularizations, such as Liu-type estimator [34], [35] and Bayesian regularization [36], [37]. Besides, there are other regularizations based on the norms other than the $L2$ norm [38], [39]. For an overall review of regularization theory and its application to inverse problems, one can refer to [40] and [41], the related numerical methods can refer to [42], and the numerical tools can refer to [43].

Both regularized solutions of the Tikhonov and TSVD methods are biased, and the bias estimates can only be computed with the estimated parameters since the true parameters are not available. With estimated biases, Xu *et al.* [44] and Xu [45] corrected the biases of the residuals and then used the bias-corrected residuals to estimate the variance components of different observations. The bias-corrected residuals are also used to construct the hypothesis tests by Li *et al.* [46]. When the absolute bias of a frequency term is larger than the reduced squared variance of this term, this term is over-regularized. For this reason, Shen *et al.* [47] derived an expression to determine the over-regularized low-frequency terms, corrected the biases to these terms to derive the bias-corrected regularized estimates that are better than the original ones in terms of MSE, and also proved that correcting the low-frequency terms means that these terms are not regularized. However, some high-frequency terms may be under-regularized for a given regularization parameter, which is not considered in [47]. Truncating these under-regularized high-frequency terms same as the TSVD method may further improve the solution since the combined use of Tikhonov and TSVD methods can get a better solution than either of the single ones, though the number of truncated parameters is empirically determined [48]. However, the low-frequency terms are still regularized in [48], and the retained medium-frequency terms after truncation are not regularized in the TSVD method. Therefore, in this article, we will develop an adaptive regularized solution for a given linear ill-posed model to improve the accuracy of estimates in terms of MSE, in which the low-, medium-, and high-frequency terms are adaptively determined, these terms are not regularized, but regularized by Tikhonov and TSVD methods.

The remaining of this article is organized as follows. In Section II, ordinary Tikhonov regularization and TSVD regularization are briefly introduced. In Section III, an adaptive regularized solution is constructed in spectral form, which adaptively combines the least-squares (LS) method, Tikhonov method, and TSVD method to derive the regularized solution with the smallest MSE; the analytical conditions are derived for determining the sets of the low-, medium-, and high-frequency terms. Also, two almost unbiased estimators of the variance of unit weight are derived to iteratively solve the unknown parameters. In Sections IV and V, a numerical example and a real geodetic example are presented to demonstrate the performance of the proposed solution and compare it with the conventional Tikhonov and TSVD regularizations. Some conclusions and remarks are summarized in Section VI.

II. Regularized Solutions to Inverse Ill-Posed Models

In the linear discrete ill-posed models

$$\boldsymbol{y} = \boldsymbol{A}\boldsymbol{x} + \boldsymbol{\varepsilon} \tag{1}$$

where $\boldsymbol{y}$ is an m vector of observations; $\boldsymbol{A}$ is an $m \times n (m > n)$ deterministic coefficient matrix, which is assumed to be full of column rank, but with singular values close to zeros; $\boldsymbol{x}$ is an n vector of unknown parameters to be estimated; and $\boldsymbol{\varepsilon}$ is the random error vector of measurements with zero mean and variance–covariance matrix $\sigma_0^2 \boldsymbol{P}^{-1}$. Here, σ_0^2 is the unknown variance of the unit weight and $\boldsymbol{P}$ is a given positive definite weight matrix. To stabilize the solution of (1), the cost function $\Phi(\boldsymbol{x})$ of Tikhonov regularization is expressed as

$$\min\colon \Phi(\boldsymbol{x}) = \|\boldsymbol{y} - \boldsymbol{A}\boldsymbol{x}\|_{\boldsymbol{P}}^2 + \alpha \|\boldsymbol{x}\|_{\boldsymbol{Q}}^2 \tag{2}$$

where $\|\cdot\|^2$ is the two-norm operator, $\boldsymbol{Q}$ is the $n \times n$ regularization matrix, and α is a positive regularization parameter. If $\boldsymbol{P}$ and $\boldsymbol{Q}$ are positive definite and decomposed as $\boldsymbol{P} = (\boldsymbol{P}^{1/2})^T \boldsymbol{P}^{1/2}$ and $\boldsymbol{Q} = (\boldsymbol{Q}^{1/2})^T \boldsymbol{Q}^{1/2}$, (1) can be transformed as

$$\boldsymbol{y}' = \boldsymbol{A}'\boldsymbol{x}' + \boldsymbol{\varepsilon}' \tag{3}$$

with $\boldsymbol{y}' = \boldsymbol{P}^{1/2}\boldsymbol{y}$, $\boldsymbol{A}' = \boldsymbol{P}^{1/2}\boldsymbol{A}\boldsymbol{Q}^{-1/2}$, and $\boldsymbol{x}' = \boldsymbol{Q}^{1/2}\boldsymbol{x}$. The cost function (2) is then rewritten as

$$\min\colon \Phi(\boldsymbol{x}') = \|\boldsymbol{y}' - \boldsymbol{A}'\boldsymbol{x}'\|_{\boldsymbol{I}_m}^2 + \alpha \|\boldsymbol{x}'\|_{\boldsymbol{I}_n}^2 \tag{4}$$

where $\boldsymbol{I}_m$ and $\boldsymbol{I}_n$ denote the $m \times m$ and $n \times n$ identity matrices, respectively. It is easily proved that the solution of (3) under the cost function (4) is equivalent to the solution of (1) under the cost function (2). Therefore, without the loss of generality, the identity weight matrix and the identity regularization matrix are adopted in the remaining of this article. The Tikhonov regularized solution of (1) is

$$\hat{\boldsymbol{x}}_\alpha = (\boldsymbol{N} + \alpha \boldsymbol{I}_n)^{-1} \boldsymbol{A}^T \boldsymbol{y} \tag{5}$$

where $\hat{\boldsymbol{x}}_\alpha$ denotes the regularized estimate, the normal matrix $\boldsymbol{N} = \boldsymbol{A}^T\boldsymbol{A}$, and the superscripts "$-1$" and "T" represent the inverse and transpose of a matrix, respectively. Apart from Tikhonov regularization, TSVD regularization is another popularly used method to solve ill-conditioned equations. By performing singular value decomposition on design matrix $\boldsymbol{A}$, we have

$$\boldsymbol{A} = \boldsymbol{U}\boldsymbol{\Lambda}\boldsymbol{V}^T = \sum_{i=1}^{n} \lambda_i \boldsymbol{u}_i \boldsymbol{v}_i^T \tag{6}$$

where $\boldsymbol{U}$ is an $m \times n$ orthogonal matrix with $\boldsymbol{U}^T\boldsymbol{U} = \boldsymbol{I}_n$, $\boldsymbol{u}_i$ is its ith column vector, $\boldsymbol{\Lambda}$ is an $n \times n$ diagonal matrix of the singular values λ_i, $\boldsymbol{V}$ is an $n \times n$ orthogonal matrix

with $\boldsymbol{V}^T\boldsymbol{V} = \boldsymbol{V}\boldsymbol{V}^T = \boldsymbol{I}_n$, and $\boldsymbol{v}_i$ is its ith column vector. The TSVD regularized solution of (1) is

$$\hat{\boldsymbol{x}}_k = \boldsymbol{A}_k^+ \boldsymbol{y} \tag{7}$$

where $\boldsymbol{A}_k = \boldsymbol{U}\boldsymbol{\Lambda}_k\boldsymbol{V}^T$, $\boldsymbol{\Lambda}_k$ is a diagonal matrix with the elements of $\lambda_1, \lambda_2, \ldots, \lambda_k, 0, \ldots, 0$, the superscript "+" denotes the Moore–Penrose inverse operator, and k is the truncation parameter.

III. Adaptive Regularized Solution

A. Parameter Estimate

By substituting (6) into (5) and (7), we can obtain the spectral decomposition form of $\hat{\boldsymbol{x}}_\alpha$ and $\hat{\boldsymbol{x}}_k$ as follows:

$$\hat{\boldsymbol{x}}_\alpha = \sum_{i=1}^{n} \frac{\lambda_i}{\lambda_i^2 + \alpha} \boldsymbol{v}_i \boldsymbol{u}_i^T \boldsymbol{y} \tag{8}$$

$$\hat{\boldsymbol{x}}_k = \sum_{i=1}^{k} \frac{1}{\lambda_i} \boldsymbol{v}_i \boldsymbol{u}_i^T \boldsymbol{y}. \tag{9}$$

By setting $\alpha = 0$ or $k = n$, regularized solutions will be degenerated into LS solutions

$$\hat{\boldsymbol{x}}_L = \sum_{i=1}^{n} \frac{1}{\lambda_i} \boldsymbol{v}_i \boldsymbol{u}_i^T \boldsymbol{y}. \tag{10}$$

We can conclude from (8) to (10) that: 1) the high-frequency terms are significantly amplified by small singular values in the LS solution; 2) the Tikhonov regularization introduces a positive regularization parameter to stabilize the high-frequency terms; and 3) the TSVD regularization directly truncates the high-frequency terms. However, there exist some drawbacks to the Tikhonov and TSVD regularizations. For Tikhonov regularization, since the low-frequency singular values are relatively larger, it may be unwise to regularize these terms. In the remaining terms to be regularized, it is of crucial importance to determine which regularization methods should be employed, i.e., Tikhonov or TSVD method. Therefore, a regularized solution reasonably consists of three parts: 1) the terms need not be regularized; 2) the terms are regularized with the Tikhonov method; and 3) the terms are regularized with the TSVD method. Hence, an adaptive regularization is constructed as

$$\hat{\boldsymbol{x}}_u = \left(\sum_{i \in S_1} \gamma_i \boldsymbol{v}_i \boldsymbol{u}_i^T + \sum_{i \in S_2} \eta_i \boldsymbol{v}_i \boldsymbol{u}_i^T + \sum_{i \in S_3} \omega_i \boldsymbol{v}_i \boldsymbol{u}_i^T \right) \boldsymbol{y} \tag{11}$$

where S_1, S_2, S_3 are the index sets and γ_i, η_i, ω_i are the corresponding coefficients for the LS method, Tikhonov regularization, and TSVD regularization, respectively. The index sets should obey the following condition:

$$\begin{aligned} &S_1 \cup S_2 \cup S_3 = \mathbb{Z} \\ &S_1 \cap S_2 = \emptyset, \quad S_1 \cap S_3 = \emptyset, \quad S_2 \cap S_3 = \emptyset \end{aligned} \tag{12}$$

in which $\mathbb{Z} = \{1, 2, \ldots, n\}$, $\emptyset$ is the empty set and the symbols "$\cup$" and "$\cap$" denote the union and intersection operators, respectively. The coefficients $\gamma_i, \eta_i, \omega_i$ are

$$\gamma_i = 1/\lambda_i, \quad \eta_i = \lambda_i / \left(\lambda_i^2 + \alpha\right), \quad \omega_i = 0. \tag{13}$$

Since $\omega_i = 0$, (11) can further be simplified as

$$\hat{\boldsymbol{x}}_u = \left(\sum_{i \in S_1} \gamma_i \boldsymbol{v}_i \boldsymbol{u}_i^T + \sum_{i \in S_2} \eta_i \boldsymbol{v}_i \boldsymbol{u}_i^T \right) \boldsymbol{y}. \tag{14}$$

It is now clear that (8)–(10) are the special cases of (14), and the solution (14) will degenerate into ordinary solutions under the conditions as follows:

$$\begin{aligned} &\hat{\boldsymbol{x}}_u \to \hat{\boldsymbol{x}}_L (S_1 = \mathbb{Z}, S_2 = \emptyset) \\ &\hat{\boldsymbol{x}}_u \to \hat{\boldsymbol{x}}_\alpha (S_1 = \emptyset, S_2 = \mathbb{Z}) \\ &\hat{\boldsymbol{x}}_u \to \hat{\boldsymbol{x}}_k (S_1 = \mathbb{Z}_k, S_2 = \emptyset) \end{aligned} \tag{15}$$

in which $\mathbb{Z}_k = \{1, 2, \ldots, k\}$. If S_1 and S_2 are determined exactly, the solution (14) is expected to perform better than conventional Tikhonov or TSVD regularization solutions. The analytical conditions for determining S_1 and S_2 are derived in Section III-B.

According to the law of error propagation, the covariance matrix of the adaptive regularized solution $\hat{\boldsymbol{x}}_u$ is derived from (14) as

$$D(\hat{\boldsymbol{x}}_u) = \sigma_0^2 \left(\sum_{i \in S_1} \frac{\boldsymbol{v}_i \boldsymbol{v}_i^T}{\lambda_i^2} + \sum_{i \in S_2} \frac{\lambda_i^2 \boldsymbol{v}_i \boldsymbol{v}_i^T}{\left(\lambda_i^2 + \alpha\right)^2} \right) \tag{16}$$

where $D(\cdot)$ denotes the dispersion operator and σ_0^2 is the (unknown) variance of unit weight. Applying the expectation to (14), we have

$$E(\hat{\boldsymbol{x}}_u) = \left(\sum_{i \in S_1} \boldsymbol{v}_i \boldsymbol{v}_i^T + \sum_{i \in S_2} \frac{\lambda_i^2}{\lambda_i^2 + \alpha} \boldsymbol{v}_i \boldsymbol{v}_i^T \right) \bar{\boldsymbol{x}} \tag{17}$$

where $E(\cdot)$ denotes the expectation operator and $\bar{\boldsymbol{x}}$ is the true values of the unknown parameters. It is obvious that the adaptive regularized solution $\hat{\boldsymbol{x}}_u$ is also biased and the biases can be computed with

$$B(\hat{\boldsymbol{x}}_u) = E(\hat{\boldsymbol{x}}_u) - \bar{\boldsymbol{x}} = -\left(\sum_{i \in S_2} \frac{\alpha}{\lambda_i^2 + \alpha} \boldsymbol{v}_i \boldsymbol{v}_i^T + \sum_{i \in S_3} \boldsymbol{v}_i \boldsymbol{v}_i^T \right) \bar{\boldsymbol{x}} \tag{18}$$

where $B(\cdot)$ denotes the bias operator. With (16) and (18), we can compute the MSE of $\hat{\boldsymbol{x}}_u$

$$\begin{aligned} M(\hat{\boldsymbol{x}}_u) &= D(\hat{\boldsymbol{x}}_u) + B(\hat{\boldsymbol{x}}_u) B^T(\hat{\boldsymbol{x}}_u) \\ &= \sum_{i \in S_1} \frac{\sigma_0^2}{\lambda_i^2} \boldsymbol{v}_i \boldsymbol{v}_i^T + \sum_{i \in S_2} \frac{\sigma_0^2 \lambda_i^2 + \alpha^2 \left(\boldsymbol{v}_i^T \bar{\boldsymbol{x}}\right)^2}{\left(\lambda_i^2 + \alpha\right)^2} \boldsymbol{v}_i \boldsymbol{v}_i^T \\ &\quad + \sum_{i \in S_3} \left(\boldsymbol{v}_i^T \bar{\boldsymbol{x}}\right)^2 \boldsymbol{v}_i \boldsymbol{v}_i^T \end{aligned} \tag{19}$$

where $M(\cdot)$ is the MSE operator.

B. Determination of S_1 and S_2

The key issue of the proposed adaptive regularization method is the determination of index sets S_1 and S_2, by which the quality of the adaptive regularized estimates is better

than the original ones. According to the law of error propagation, the covariance matrix of LS solution $\hat{\boldsymbol{x}}_L$ is derived from (10) as

$$\boldsymbol{D}(\hat{\boldsymbol{x}}_L) = \sigma_0^2 \sum_{i=1}^{n} \frac{\boldsymbol{v}_i \boldsymbol{v}_i^T}{\lambda_i^2} \tag{20}$$

and the covariance matrices of the Tikhonov regularized estimate and TSVD estimate are derived, respectively, from (8) and (9) as

$$\boldsymbol{D}(\hat{\boldsymbol{x}}_\alpha) = \sigma_0^2 \sum_{i=1}^{n} \frac{\lambda_i^2 \boldsymbol{v}_i \boldsymbol{v}_i^T}{\left(\lambda_i^2 + \alpha\right)^2} \tag{21}$$

$$\boldsymbol{D}(\hat{\boldsymbol{x}}_k) = \sigma_0^2 \sum_{i=1}^{k} \frac{\boldsymbol{v}_i \boldsymbol{v}_i^T}{\lambda_i^2}. \tag{22}$$

Since the Tikhonov and TSVD solutions are biased, the biases of the solutions are estimated as

$$\boldsymbol{B}(\hat{\boldsymbol{x}}_\alpha) = -\sum_{i=1}^{n} \frac{\alpha}{\lambda_i^2 + \alpha} \boldsymbol{v}_i \boldsymbol{v}_i^T \bar{\boldsymbol{x}} \tag{23}$$

$$\boldsymbol{B}(\hat{\boldsymbol{x}}_k) = -\sum_{i=k+1}^{n} \boldsymbol{v}_i \boldsymbol{v}_i^T \bar{\boldsymbol{x}}. \tag{24}$$

The MSEs of Tikhonov and TSVD estimates are

$$\begin{aligned} \boldsymbol{M}(\hat{\boldsymbol{x}}_\alpha) &= \boldsymbol{D}(\hat{\boldsymbol{x}}_\alpha) + \boldsymbol{B}(\hat{\boldsymbol{x}}_\alpha)\boldsymbol{B}(\hat{\boldsymbol{x}}_\alpha)^T \\ &= \sigma_0^2 \sum_{i=1}^{n} \frac{\lambda_i^2 \boldsymbol{v}_i \boldsymbol{v}_i^T}{\left(\lambda_i^2 + \alpha\right)^2} + \alpha^2 \sum_{i=1}^{n} \frac{\left(\boldsymbol{v}_i^T \bar{\boldsymbol{x}}\right)^2 \boldsymbol{v}_i \boldsymbol{v}_i^T}{\left(\lambda_i^2 + \alpha\right)^2} \end{aligned} \tag{25}$$

$$\begin{aligned} \boldsymbol{M}(\hat{\boldsymbol{x}}_k) &= \boldsymbol{D}(\hat{\boldsymbol{x}}_k) + \boldsymbol{B}(\hat{\boldsymbol{x}}_k)\boldsymbol{B}(\hat{\boldsymbol{x}}_k)^T \\ &= \sigma_0^2 \sum_{i=1}^{k} \frac{\boldsymbol{v}_i \boldsymbol{v}_i^T}{\lambda_i^2} + \sum_{i=k+1}^{n} \left(\boldsymbol{v}_i^T \bar{\boldsymbol{x}}\right)^2 \boldsymbol{v}_i \boldsymbol{v}_i^T. \end{aligned} \tag{26}$$

Therefore, the traced MSE reduction of Tikhonov regularized solution relative to LS solution as

$$\begin{aligned} \Delta T_{\alpha L} &= \mathrm{Tr}(\boldsymbol{D}(\hat{\boldsymbol{x}}_L)) - \mathrm{Tr}(\boldsymbol{M}(\hat{\boldsymbol{x}}_\alpha)) \\ &= \alpha^2 \sum_{i=1}^{n} \frac{\sigma_0^2\left(\frac{2}{\alpha} + \frac{1}{\lambda_i^2}\right) - \left(\boldsymbol{v}_i^T \bar{\boldsymbol{x}}\right)^2}{\left(\lambda_i^2 + \alpha\right)^2}. \end{aligned} \tag{27}$$

Similarly, the traced MSE reduction of TSVD solution relative to the LS solution as

$$\Delta T_{kL} = \mathrm{Tr}(\boldsymbol{D}(\hat{\boldsymbol{x}}_L)) - \mathrm{Tr}(\boldsymbol{M}(\hat{\boldsymbol{x}}_k)) = \sum_{i=k+1}^{n} \left(\frac{\sigma_0^2}{\lambda_i^2} - \left(\boldsymbol{v}_i^T \bar{\boldsymbol{x}}\right)^2\right). \tag{28}$$

As shown in the right-hand side of (27) and (28), there is no guarantee that each frequency component is greater than zero. For the Tikhonov regularization, the terms satisfying the following condition should not be regularized:

$$\sigma_0^2\left(\frac{2}{\alpha} + \frac{1}{\lambda_i^2}\right) \le \left(\boldsymbol{v}_i^T \bar{\boldsymbol{x}}\right)^2. \tag{29}$$

Also, for the TSVD method, the terms satisfying the condition (30) should not be regularized

$$\frac{\sigma_0^2}{\lambda_i^2} \le \left(\boldsymbol{v}_i^T \bar{\boldsymbol{x}}\right)^2. \tag{30}$$

Obviously, the terms that satisfy (29) will also satisfy (30). Therefore, the set S_1 is determined by

$$S_1 = \left\{ i \,|\, \sigma_0^2\left(\frac{2}{\alpha} + \frac{1}{\lambda_i^2}\right) \le \left(\boldsymbol{v}_i^T \bar{\boldsymbol{x}}\right)^2 \right\}. \tag{31}$$

The remaining task is to determine the set S_2, i.e., the terms that should be regularized by the Tikhonov method instead of the TSVD method. Since both two regularizations can effectively reduce the MSE of solutions in different ways, we can compare their reductions with respect to the LS solution. According to (27), by introducing the regularization parameter α, the MSE reduction of $\hat{\boldsymbol{x}}_\alpha$ with respect to $\hat{\boldsymbol{x}}_L$ for each component is

$$\Delta T_\alpha^i = \alpha^2 \frac{\sigma_0^2\left(\frac{2}{\alpha} + \frac{1}{\lambda_i^2}\right) - \left(\boldsymbol{v}_i^T \bar{\boldsymbol{x}}\right)^2}{\left(\lambda_i^2 + \alpha\right)^2} \tag{32}$$

while for TSVD regularization, by truncating the ith component, the MSE reduction of $\hat{\boldsymbol{x}}_k$ with respect to $\hat{\boldsymbol{x}}_L$ is

$$\Delta T_k^i = \frac{\sigma_0^2}{\lambda_i^2} - \left(\boldsymbol{v}_i^T \bar{\boldsymbol{x}}\right)^2. \tag{33}$$

Hence, the traced MSE reduction of TSVD solution relative to the Tikhonov solution is derived from (32) and (33) as

$$\begin{aligned} \Delta T_{k\alpha} &= \Delta T_\alpha^i - \Delta T_k^i \\ &= \frac{\lambda_i^2\left(\lambda_i^2 + 2\alpha\right)}{\left(\lambda_i^2 + \alpha\right)^2}\left(\left(\boldsymbol{v}_i^T \bar{\boldsymbol{x}}\right)^2 - \frac{\sigma_0^2}{\lambda_i^2 + 2\alpha}\right). \end{aligned} \tag{34}$$

It is now clear from (34) that only the terms satisfying (35) are suitable for Tikhonov regularization; otherwise, they are suitable for TSVD regularization

$$\left(\boldsymbol{v}_i^T \bar{\boldsymbol{x}}\right)^2 > \frac{\sigma_0^2}{\lambda_i^2 + 2\alpha}. \tag{35}$$

Therefore, the set S_2 is determined with

$$S_2 = \left\{ i \,|\, \frac{\sigma_0^2}{\lambda_i^2 + 2\alpha} < \left(\boldsymbol{v}_i^T \bar{\boldsymbol{x}}\right)^2 < \sigma_0^2\left(\frac{2}{\alpha} + \frac{1}{\lambda_i^2}\right) \right\}. \tag{36}$$

By simple algebraic derivations, the sets S_1 and S_2 in (31) and (36) can be written as

$$S_1 = \left\{ i \,|\, \lambda_i^2 \ge \frac{\alpha\sigma_0^2}{\alpha\left(\boldsymbol{v}_i^T \bar{\boldsymbol{x}}\right)^2 - 2\sigma_0^2} \right\} \tag{37}$$

$$S_2 = \left\{ i \,|\, \frac{\sigma_0^2}{\left(\boldsymbol{v}_i^T \bar{\boldsymbol{x}}\right)^2} - 2\alpha < \lambda_i^2 < \frac{\alpha\sigma_0^2}{\alpha\left(\boldsymbol{v}_i^T \bar{\boldsymbol{x}}\right)^2 - 2\sigma_0^2} \right\}. \tag{38}$$

It is now obvious from (37) and (38) that some low-frequency terms relative to large singular values should not be regularized, and some high-frequency terms should be truncated; only the medium-frequency terms should be regularized by the Tikhonov regularization.

C. Estimation of the Unit Weight Variance

To determine the sets S_1 and S_2 with (31) and (36), the true values of parameters and unit weight variance should be known in advance. However, this is unrealistic; otherwise, we do not need to solve the model. Fortunately, we can replace $\bar{\boldsymbol{x}}$ and σ_0^2 with their estimates $\hat{\boldsymbol{x}}_u$ and $\hat{\sigma}_0^2$ in (31) and (36). Since the determination of S_1 and S_2 and the estimation of unknown parameters are involved with each other, the proposed algorithm should be performed iteratively. To minimize the impact of bias of the unit weight variance estimate on the determination of S_1 and S_2, we have derived two almost unbiased estimators of $\hat{\sigma}_0^2$ with the adaptive regularized solution $\hat{\boldsymbol{x}}_u$ for each iteration. First, we give the following equation:

$$E\left(\hat{\boldsymbol{e}}^T\hat{\boldsymbol{e}}\right) = \mathrm{tr}(D(\hat{\boldsymbol{e}})) + E(\hat{\boldsymbol{e}})^T E(\hat{\boldsymbol{e}}). \tag{39}$$

Equation (39) builds the connection between the residual and the unit weight variance. Substituting (14) into (1), we will derive the following expression of computing residuals:

$$\hat{\boldsymbol{e}}_u = \left(\boldsymbol{I}_m - \sum_{i\in S_1}\boldsymbol{u}_i\boldsymbol{u}_i^T - \sum_{i\in S_2}\frac{\lambda_i^2}{\lambda_i^2+\alpha}\boldsymbol{u}_i\boldsymbol{u}_i^T\right)\boldsymbol{y}. \tag{40}$$

The expectation and variance–covariance matrix of $\hat{\boldsymbol{e}}_u$ are

$$E(\hat{\boldsymbol{e}}_u) = \left(\alpha\sum_{i\in S_2}\frac{\lambda_i}{\lambda_i^2+\alpha}\boldsymbol{u}_i\boldsymbol{v}_i^T + \sum_{i\in S_3}\lambda_i\boldsymbol{u}_i\boldsymbol{v}_i^T\right)\bar{\boldsymbol{x}} \tag{41}$$

$$D(\hat{\boldsymbol{e}}_u) = \sigma_0^2\left(\boldsymbol{I}_m - \sum_{i\in S_1\cup S_2}\boldsymbol{u}_i\boldsymbol{u}_i^T + \alpha^2\sum_{i\in S_2}\frac{1}{\left(\lambda_i^2+\alpha\right)^2}\boldsymbol{u}_i\boldsymbol{u}_i^T\right). \tag{42}$$

Substituting (41) and (42) into (39) and removing the expectation operator of the left-hand side, after some simple algebraic derivations, we have

$$\hat{\sigma}_0^2 = \frac{\hat{\boldsymbol{e}}_u^T\hat{\boldsymbol{e}}_u - \alpha^2\sum_{i\in S_2}\frac{\lambda_i^2}{\left(\lambda_i^2+\alpha\right)^2}\left(\boldsymbol{v}_i^T\bar{\boldsymbol{x}}\right)^2 - \sum_{i\in S_3}\lambda_i^2\left(\boldsymbol{v}_i^T\bar{\boldsymbol{x}}\right)^2}{m - m_{S_1} - m_{S_2} + \alpha^2\sum_{i\in S_2}\left(\lambda_i^2+\alpha\right)^{-2}} \tag{43}$$

where m_{S_1} and m_{S_2} are the numbers of elements belonging to the sets S_1 and S_2, respectively. The estimator given by (43) is strictly unbiased in the presence of $\bar{\boldsymbol{x}}$. Since $\bar{\boldsymbol{x}}$ is generally unknown in practical applications, we replace it with the adaptive regularized solution $\hat{\boldsymbol{x}}_u$. On the other hand, we can also correct the bias of the residual and then use the bias-corrected residual to compute the unit weight variance [44]. By replacing $\bar{\boldsymbol{x}}$ with $\hat{\boldsymbol{x}}_u$ in (41), we can obtain the bias estimate of residual as

$$\hat{E}(\hat{\boldsymbol{e}}_u) = \sum_{i\in S_2}\frac{\lambda_i^2\alpha}{\left(\lambda_i^2+\alpha\right)^2}\boldsymbol{u}_i\boldsymbol{u}_i^T\boldsymbol{y}. \tag{44}$$

Subtracting $\hat{E}(\hat{\boldsymbol{e}}_u)$ from $\hat{\boldsymbol{e}}_u$, we can obtain the bias-corrected residual with

$$\begin{aligned}\bar{\boldsymbol{e}}_u &= \hat{\boldsymbol{e}}_u - \hat{E}(\hat{\boldsymbol{e}}_u)\\ &= \left(\boldsymbol{I}_m - \sum_{i\in S_1}\boldsymbol{u}_i\boldsymbol{u}_i^T - \sum_{i\in S_2}\frac{\lambda_i^2\left(\lambda_i^2+2\alpha\right)}{\left(\lambda_i^2+\alpha\right)^2}\boldsymbol{u}_i\boldsymbol{u}_i^T\right)\boldsymbol{y}.\end{aligned} \tag{45}$$

Substituting (45) into (39) and after a lengthy derivation, we can obtain another almost unbiased estimate of the unit weight variance

$$\hat{\sigma}_0^2 = \frac{\bar{\boldsymbol{e}}_u^T\bar{\boldsymbol{e}}_u}{m - m_{S_1} - m_{s_2} + \alpha^4\sum_{i\in S_2}\left(\lambda_i^2+\alpha\right)^{-4}}. \tag{46}$$

In practical computation, the difference between two estimators is really small, and the readers can choose any of them to estimate the variance of the unit weight. In ordinary regularization, the regularization parameter is committed to regularizing the terms of all frequencies, while in our adaptive regularization, the regularization parameter is only responsible for the medium-frequency terms. Since several high-frequency terms are truncated in adaptive regularization, the regularization parameter should be updated (See Appendix A) and smaller than the ordinary one. However, in practice, the regularization parameters calculated with the regularized solutions tend to be overestimated since the regularized estimates have a smaller power spectrum than the true values [47]. To avoid such an overestimation of the regularization parameter, we impose the following constraint:

$$\alpha_u < \alpha_r \tag{47}$$

where α_u and α_r denote the regularization parameters for adaptive regularization and ordinary regularization, respectively. The flowchart of the algorithm for computing the adaptive regularized solution to ill-posed models is presented in Appendix B.

IV. Numerical Example

A. Criteria for Comparison of Results

In this section, we design a numerical example to demonstrate the performance of the proposed adaptive regularized solution and compare it with ordinary Tikhonov and TSVD regularized solutions. The mean MSE root is employed to compare different regularized solutions, which is defined as

$$\mathrm{mmr} = \sqrt{\frac{1}{n}\mathrm{Tr}(\boldsymbol{M})} \tag{48}$$

where $\boldsymbol{M}$ denotes the MSE matrix of regularized solution and n is the number of unknown parameters. As can be seen from (19), the computation of MSE requires the true parameters that are known for a simulated example. However, the true parameters are impossibly known in practical applications and only their estimates can be obtained. To this end, we also compute the MSE with the corresponding regularized estimates. Moreover, since the simulation results can be repeated and the true parameters are also known, the MSE can be computed numerically as follows:

$$\boldsymbol{M}_E = \frac{1}{N}\sum_{i=1}^{N}(\hat{\boldsymbol{x}}-\bar{\boldsymbol{x}})^T(\hat{\boldsymbol{x}}-\bar{\boldsymbol{x}}) \tag{49}$$

where $\boldsymbol{M}_E$ denotes the numerically estimated MSE of the parameter estimates, N is the number of repeated experiments, and $\hat{\boldsymbol{x}}$ and $\bar{\boldsymbol{x}}$ represent the regularized estimates and true parameters, respectively. In summary, the MSE can be

estimated via three approaches: 1) the theoretical formula with the true parameters; 2) the theoretical formula with the estimates; and 3) the numerical method via repeated simulations. These three MSE values are called true, estimated, and numerically computed MSEs in the remainder of this article and abbreviated as TMSE, EMSE, and NMSE, respectively. For convenience, we abbreviate the ordinary Tikhonov regularized solution, TSVD regularized solution, and iterative adaptive regularized solution as OTiko, OTsvd, and ITada, respectively. Furthermore, to illustrate the performance of the proposed method incrementally, we also compute the partially Tikhonov regularized solution (PTiko), which is computed by replacing S_2 with $\bar{S}_1 = \mathbb{Z} - S_1$ in (14) and the initial adaptive regularized solution (INada) by (14), in which the regularization parameter is not updated. To ensure a fair comparison of various approaches, the regularization parameter and truncation parameter are all determined based on the minimum MSE criteria [26], [27], [28], [33]. The initial regularization parameter for adaptive regularization is the same as the counterpart for pure Tikhonov regularization.

B. Fredholm Integral Equation of the First Kind

The Fredholm integral equation of the first kind is a typical ill-posed model and is commonly used in geodetic and remote sensing inversion problems, such as linear ground penetrating radar (GPR) inversion [49], the nuclear magnetic resonance (NMR) echo data inversion [50], and microwave inversion of leaf area and inclination angle distributions [51]. Its general form is

$$z(y) = \int_a^b k(x, y) f(x) dx \tag{50}$$

where $z(y)$ is observable, $k(x, y)$ is a given kernel function, and $f(x)$ is to be estimated via the integral equation. Considering that the comparison of different regularizations does not depend on the specific form of $k(x, y)$ and $f(x)$. We employ the 1-D numerical case first proposed by Tikhonov *et al.* [42], in which the kernel function and the exact function are, respectively, expressed as

$$\begin{aligned} k(x, y) &= \frac{1}{1 + 100(y - x)^2} \\ f(x) &= \frac{e^{-(x-0.3)^2/0.03} + e^{-(x-0.7)^2/0.03}}{10.9550408} - 0.052130913. \end{aligned} \tag{51}$$

For numerical simulations, both the variables x and y are calculated at a sampling interval of 0.02 over $x \in [0, 1]$ and $y \in [-2, 2]$, respectively. $z(y)$ is numerically integrated from (50). The random error with zero mean and standard deviation of 0.001 is added to the computed $z(y)$. The discretized version of the integral in (50) is seriously ill-posed with a condition number of 10^{12}. Hence, regularized methods should be employed to stabilize the solution. According to the minimum MSE criteria, the regularization parameter and truncation parameter for Tikhonov and TSVD regularizations are determined as $\alpha = 0.0015$, $k = 6$, and thus, we obtain the OTiko solution $\hat{\boldsymbol{x}}_\alpha$ and OTsvd solution $\hat{\boldsymbol{x}}_k$. To determine

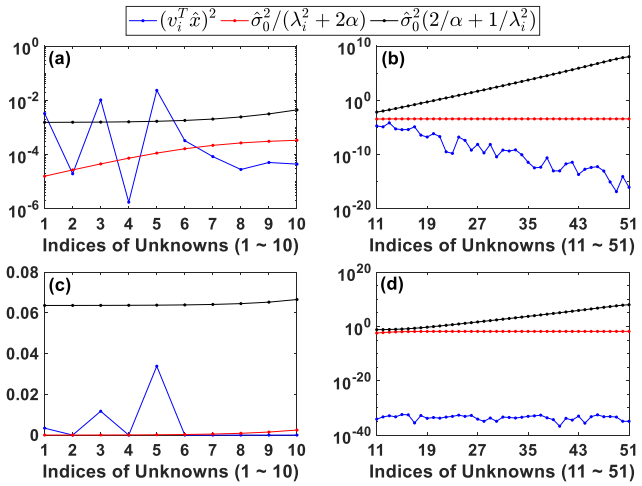

Fig. 1. Determine the index sets S_1 and S_2 using (31) and (36). (a) and (b) INada solution. (c) and (d) ITada solution.

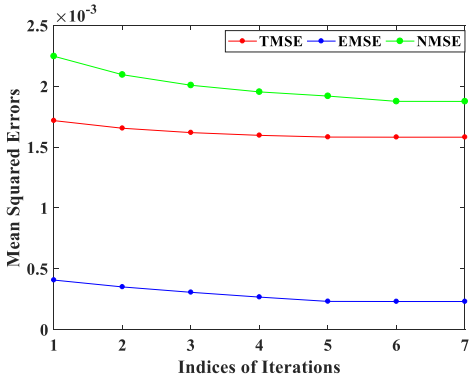

Fig. 2. MSEs of adaptive regularized solutions under different iterations.

the terms S_1 and S_2, we compute three terms $(\boldsymbol{v}_i^T \hat{\boldsymbol{x}}_\alpha)^2$, $\hat{\sigma}_0^2/(\lambda_i^2 + 2\alpha)$, and $\hat{\sigma}_0^2(2/\alpha + 1/\lambda_i^2)$ over all frequencies, and the results are presented in Fig. 1, where Fig. 1(a) and (b) are for INada solution and Fig. 1(c) and (d) are for ITada solution.

From Fig. 1, we can observe that the terms sets are different for INada solution and ITada solution, with $S_1 = \{1, 3, 5\}$ and $S_2 = \{6\}$ for the former and $S_1 = \emptyset$ and $S_2 = \{1, 3, 5\}$ for the latter. Fig. 2 shows the MSEs of adaptive regularized solutions under different iterations. It is clear that the MSEs are gradually reduced as the number of iterations increases. In practical applications, only the EMSE can be obtained since the other two indicators require the true values of unknown parameters $\overline{\boldsymbol{x}}$. The condition for terminating the iteration is that $|\Delta\text{EMSE}_{i+1}| < \delta$, where $\Delta\text{EMSE}_{i+1} = \text{EMSE}_{i+1} - \text{EMSE}_i$ and δ is a given threshold, which is set to 10^{-7} in this example. The five regularized solutions and true parameters are presented in Fig. 3(a), and the MSE roots of regularized estimates are shown in Fig. 3(b)–(d). The results clearly demonstrate that all regularized solutions are well consistent with the true values, and the proposed iterative adaptive regularized solution performs the best. Since some low-frequency terms belonging to S_1 should not be regularized, the PTiko solution performs better than the OTiko solution. On the contrary, some high-frequency terms belonging to S_3 should be truncated, and hence, the INada solution outperforms the PTiko solution. Bearing in mind that the regularization parameter for the

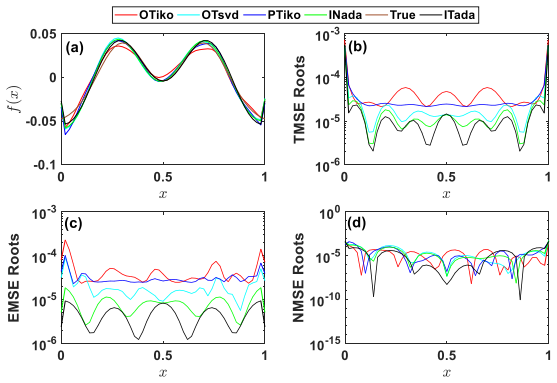

Fig. 3. Five regularized solutions and MSEs. (a) Regularized solutions and true values. (b) TMSEs. (c) EMSEs. (d) NMSEs.

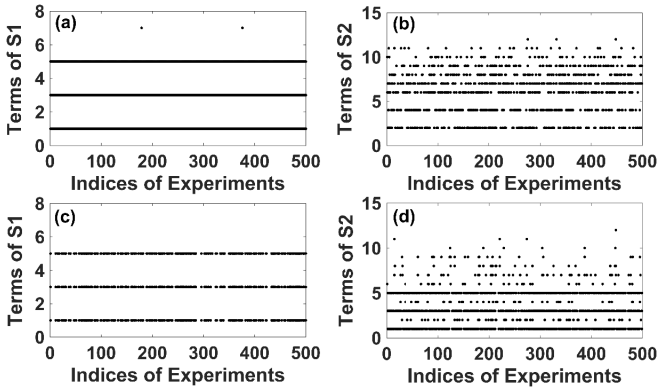

Fig. 4. Index sets S_1 and S_2 determined with (31) and (36). (a) and (b) Inada solution. (c) and (d) ITada solution.

INada solution is inherited from the OTiko solution, while the counterpart for the ITada solution is iteratively updated with minimum MSE criteria, thus, the ITada solution outperforms the INada solution.

To obtain statistically reliable results, the simulation has been repeated 500 times. The index sets S_1 and S_2 determined by (31) and (36) for the INada solution and ITada solution are presented in Fig. 4. As expected, the terms of S_1 are mainly distributed in the low-frequency region and the terms of S_2 are mainly distributed in the medium-frequency region. Since the distribution of elements in S_1 and S_2 is not consecutive in space, it is unreasonable to simply take two critical thresholds to divide the terms. The regularization parameters for OTiko solution and ITada solution and truncation parameters for OTsvd solution are shown in Fig. 5. The iteration numbers of adaptive regularization for 500 simulations are presented in Fig. 6. By using theoretical formulas or numerical simulations, we can obtain the MSEs of five regularized solutions and present them in Figs. 7 and 8.

As expected, the accuracy of regularized estimates has been progressively improved by overcoming the over-regularization of some low-frequency terms and under-regularization of some high-frequency terms. Among them, the improvements of PTiko solution relative to OTiko solution are 12.66%, 13.85%, and 13.75% in the sense of TMSE, EMSE, and NMSE, respectively; the improvements of INada solution relative to PTiko solution for TMSE, EMSE, and NMSE are 14.49%, 42.86%, and 5.80%, respectively. By iteratively updating the

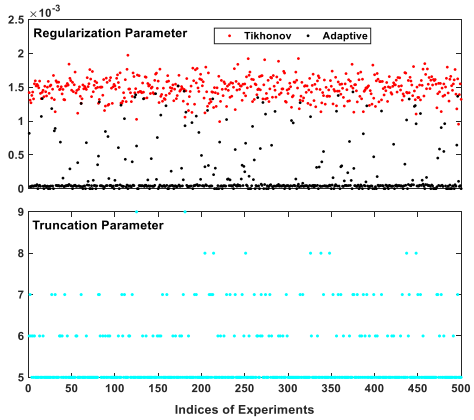

Fig. 5. Regularization parameters for OTiko and ITada solutions and truncation parameters for OTsvd solutions determined with minimum MSE criteria.

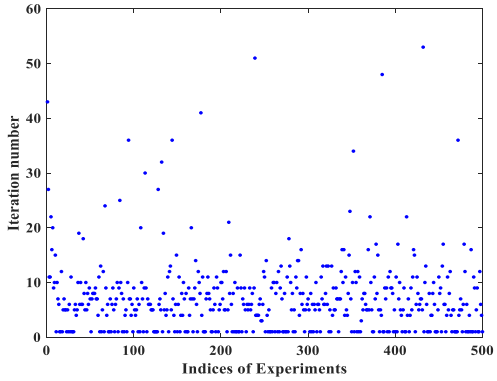

Fig. 6. Iteration numbers of adaptive regularization for 500 simulations.

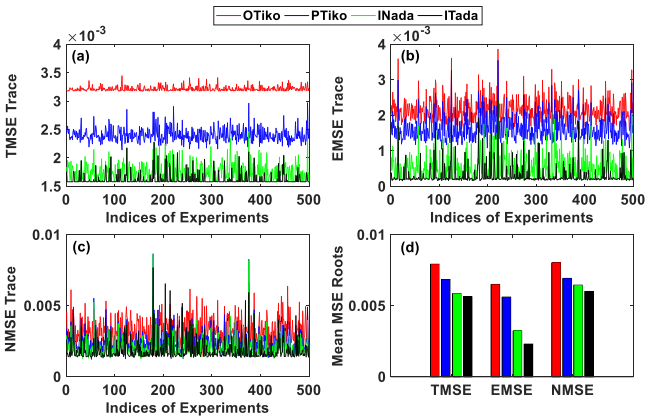

Fig. 7. MSEs of OTiko solution, PTiko solution, INada solution, and ITada solution over 500 simulations. (a) TMSE. (b) EMSE. (c) NMSE. (d) Means of MSE roots.

regularization parameters, the ITada solution can achieve a better solution than the INada solution, with the TMSE, EMSE, and NMSE reductions of about 5.08%, 28.13%, and 7.69%, respectively. In summary, our adaptive regularization can greatly improve the accuracy of the solutions to ill-posed models compared with the ordinary Tikhonov regularization, with improvements of about 29.11%, 64.62%, and 25.00% in terms of TMSE, EMSE, and NMSE. Fig. 8 also shows that the adaptive regularized solution outperforms the TSVD regularized solution, with the TMSE, EMSE, and NMSE reductions of about 6.67%, 20.69%, and 9.09%, respectively.

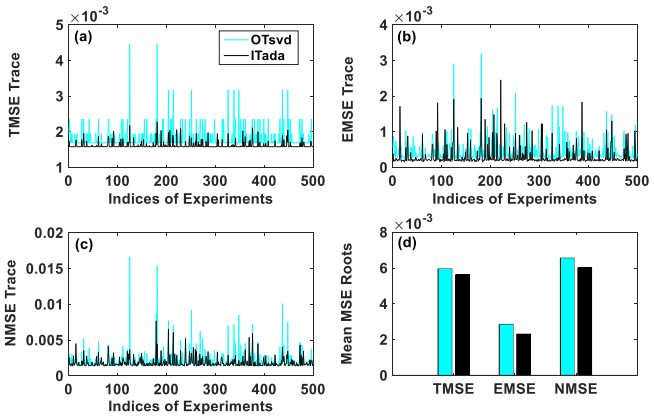

Fig. 8. MSEs of OTsvd solution and ITada solution over 500 simulations. (a) TMSE. (b) EMSE. (c) NMSE. (d) Means of MSE roots over 500 simulations.

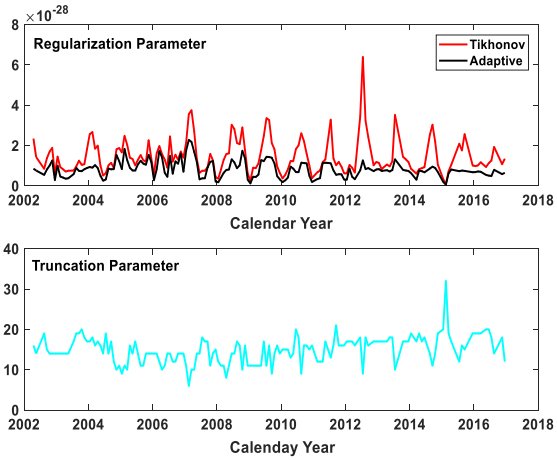

Fig. 9. Regularization parameters and truncation parameters based on minimum MSE criteria.

It can be seen from Fig. 6 that the iteration numbers for some cases are 1, indicating that the adaptive regularization may converge to the initial values. Nevertheless, the ITada solutions still perform better than OTiko and OTsvd solutions, with mean NMSE reductions of 36.36% and 4.54%, respectively.

V. Real Example

A. Mathematical Model and Data

The GRACE data have been widely used to investigate regional or global mass inversion [52], [53], [54], [55]. To further demonstrate the performance of our adaptive regularization method for geoscience applications, we apply the new method to retrieve the mass variation of the Yangtze River from April 2002 to December 2016 based on the mascon model. In mascon modeling, it is common to compute the pseudo-observables with the spherical harmonic coefficients over the region of interest. If the Earth's elastic yielding is considered, the radial gravity disturbance can be expressed as follows:

$$\delta g = -\frac{GM}{r^2}\sum_{l=2}^{l_{\max}}\left(\frac{a}{r}\right)^l \frac{(l+1)}{\left(1+k_l'\right)}\sum_{m=0}^{l} P_{lm}(\sin\varphi) \times\left(\Delta C_{lm}\cos m\lambda + \Delta S_{lm}\sin m\lambda\right) \quad (52)$$

where G is the Newton gravitational constant; r, λ, and φ are the spherical coordinates of the pseudo-observations (radius, longitude, and latitude, respectively); a is the mean radius of the Earth; l and m denote the degree and order of the gravity field, respectively; $l_{\max}$ is the maximum degree; k_l' is the load Love number of degree l; P_{lm} represents the fully normalized associated Legendre functions; and ΔC_{lm} and ΔS_{lm} are the Stokes coefficients after removing the mean gravity field. According to Newton's law of gravity, the radial gravity disturbance $\delta g_i (i = 1, 2, \ldots, m)$ at the satellite's attitude can be represented as

$$\delta g_i = G\sum_{j=1}^{n}\frac{\delta m_j}{\left(a^2+r^2-2ar\cos\psi_{i,j}\right)^{1/2}}, \quad i = 1, 2, \ldots, m \quad (53)$$

where $\delta m_j (j = 1, 2, \ldots, n)$ stands for the mass variations on the Earth's surface. With (52) and (53), we can obtain the mascon model as (1), with the unknown parameters $\boldsymbol{x} = (\delta m_1, \delta m_2, \ldots, \delta m_n)^T$ and the design matrix as

$$\boldsymbol{A}(i, j) = G\frac{1}{\left(a^2+r^2-2ar\cos\psi_{i,j}\right)^{1/2}}, \quad i = 1, 2, \ldots, m,\ j = 1, 2, \ldots, n. \quad (54)$$

The study area Yangtze River Basin is within the rectangle frame (85°E–128°E, 24°N–46°N) (see Fig. 12). Within the area, a mascon grid at 0.5° resolution with 3915 mascons is constructed. The condition number of the normal matrix is 3.18×10^{21}, and hence, it must be regularized. The Tongji-Grace 2018 monthly gravity field solutions from April 2002 to December 2016 (157 months) [11] are used in this study. The datasets can be downloaded by the International Centre for Global Earth Models (ICGEM) (http://icgem.gfz-potsdam.de/series/03_other/Tongji/Tongji-Grace2018). Since the GRACE solutions refer to the center of mass, the degree-1 coefficients of spherical harmonics have to be added back to correct the offset between the center of mass and the center of the Earth frame. Here, we corrected the offset with the degree-1 coefficients derived by satellite laser ranging (SLR) observations [56]. Considering that the C_{20} terms are poorly observed by GRACE, especially in the months with only a single accelerometer, we replace them with the counterparts provided by SLR observations [57], [58]. To enable an interpretation in terms of hydrology, the glacial isostatic adjustment (GIA) should be removed from surface mass variations. We use the ICE6G-D model [59] to correct the mascon solutions.

B. Results Analysis

The three regularizations are used to compute 3915 mascon parameters for 157 months, and the regularization parameters and truncation parameters are determined with minimum MSE criteria. As shown in Fig. 9, the regularization parameters of our adaptive regularized method are smaller than those of the ordinary Tikhonov method. The truncation parameters for TSVD regularization are approximately

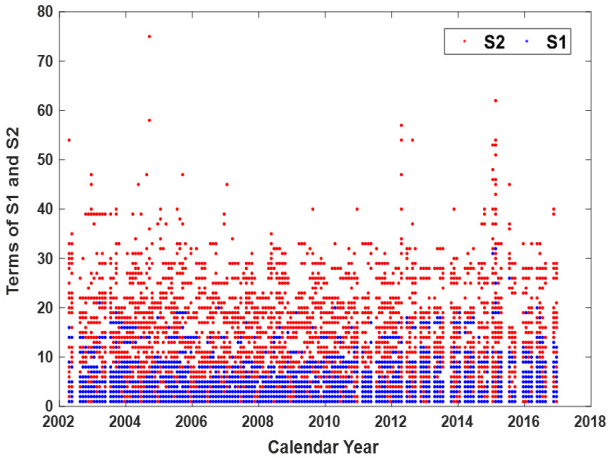

Fig. 10. Terms S_1 and S_2 computed with (31) and (36).

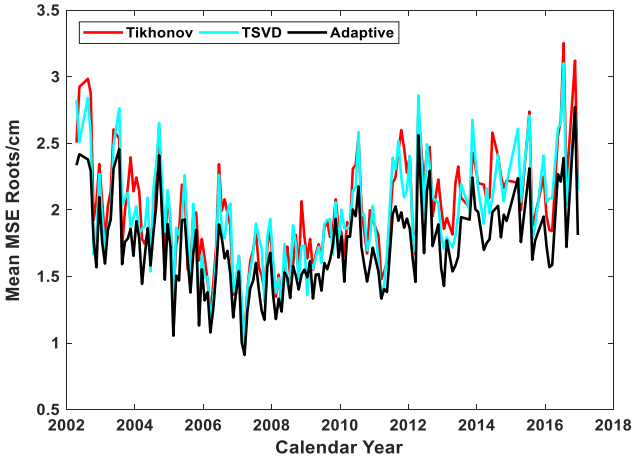

Fig. 11. Mean MSE roots of three regularized solutions for 157 months.

TABLE I
MEAN MSE ROOTS OF THREE REGULARIZED SOLUTIONS

	Mean MSE Roots (cm)		
Methods	Maximum	Minimum	Mean
Tikhonov	3.2533	1.0668	1.9811
TSVD	3.1016	0.9940	1.9428
Adaptive	2.7733	0.9106	1.7155

between 10 and 40. According to (31) and (36), the index sets S_1 and S_2, accounting for the terms that are (not) worthy of regularization, are presented in Fig. 10. It is obvious that some low-frequency terms are not worthy of regularization, and many high-frequency terms should be directly truncated. In order to compare the performance of different regularization methods, we compute the mean MSE roots of three regularized solutions for 157 months. Since the true mascon parameters are unknown, we use the regularized estimates to compute the MSE, and the results are presented in Fig. 11, where the MSEs of our adaptive regularized solutions are smaller than those of Tikhonov and TSVD regularized solutions. The means of MSE roots have been successfully reduced from 1.9811 and 1.9428 cm in the case of Tikhonov and TSVD regularizations to 1.7155 cm in the case of our adaptive regularization (Table I), with the reductions of about 13.41% and 11.70%, respectively. To better visualize the MSEs of three regularizations, we also present the spatial distribution of average MSEs of all mascons for 157 months in Fig. 12. As expected, our method can effectively improve the accuracy of mascon parameters in terms of MSE compared with the other two regularizations.

With 157 months of estimated mass flux in hand, we can compute the secular trend of mass variation in the Yangtze River Basin for three regularizations, and the results are presented in Fig. 13, among which P4M6 + 300 km Gaussian filtering, Tikhonov regularization, adaptive regularization, and TSVD regularization. It is clear that the regularized solutions are close to the filtering results, especially in the upstream and midstream, where they show a significant loss and increase of regional mass, respectively. A mass loss signal in the northwest is due to the leakage of the glacier mass loss in the Qinghai–Tibet Plateau and a significantly increased signal in the middle of the Yangtze River basin is due to three Gorges reservoir impounding [60], [61], [62]. Furthermore, Fig. 13(c) shows that our adaptive regularized solution can retain more stronger and significant signals compared with the filtering solution and Tikhonov regularized solution. For example, the maximum trend of midstream from our adaptive regularized solution is 1.05 cm/year, which is higher than 0.98 cm/year of filtering solution and 0.98 cm/year of Tikhonov regularized solution. It can be seen from Fig. 13(d) that TSVD regularization can also obtain a significant signal, and however, it will also bring visible stripes. For Tikhonov regularization, although some low-frequency terms and high-frequency terms are, respectively, suffered from over-regularization and under-regularization, the medium-frequency terms are benefitted from appropriate regularization. Hence, Tikhonov regularized solutions are smoother than TSVD regularized solutions. For TSVD regularization, although the low-frequency signal can be effectively retained and the high-frequency noise is suppressed, it may lack an effective mechanism for processing the medium-frequency terms. For example, as can be seen from Figs. 9 and 10, TSVD regularization suggests that the terms between 20 and 30 should be truncated, while our adaptive regularization demonstrates that these terms should be regularized by the Tikhonov regularization. From the spectral point of view, these medium-frequency terms may contain useful information for the parameters, which should not be simply truncated. In other words, only with a truncation term determined with minimum MSE criteria, the signal component and noise component may not be well distinguished. Our adaptive regularization approach can effectively overcome the over-regularization of some low-frequency terms and the under-regularization of some high-frequency terms, and hence, it can balance the Tikhonov and TSVD regularizations and performs the best.

To investigate the total mass variation, we compute the mass flux time series with the area-weighted average method and present them in Fig. 14(a), as well as their power spectral density (PSD) in Fig. 14(b) with the Lomb–Scargle

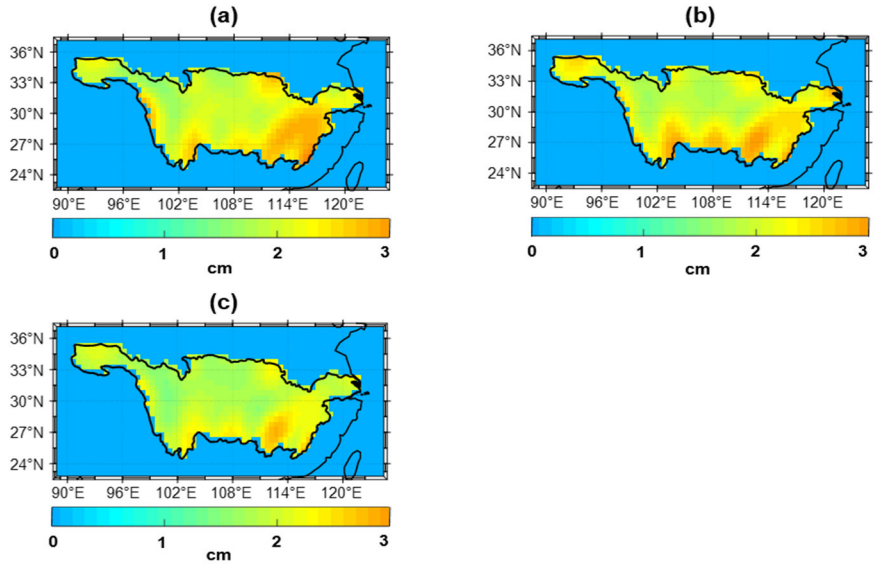

Fig. 12. Spatial distribution of average MSEs of all mascons for three regularizations. (a) Tikhonov regularization. (b) TSVD regularization. (c) Adaptive regularization.

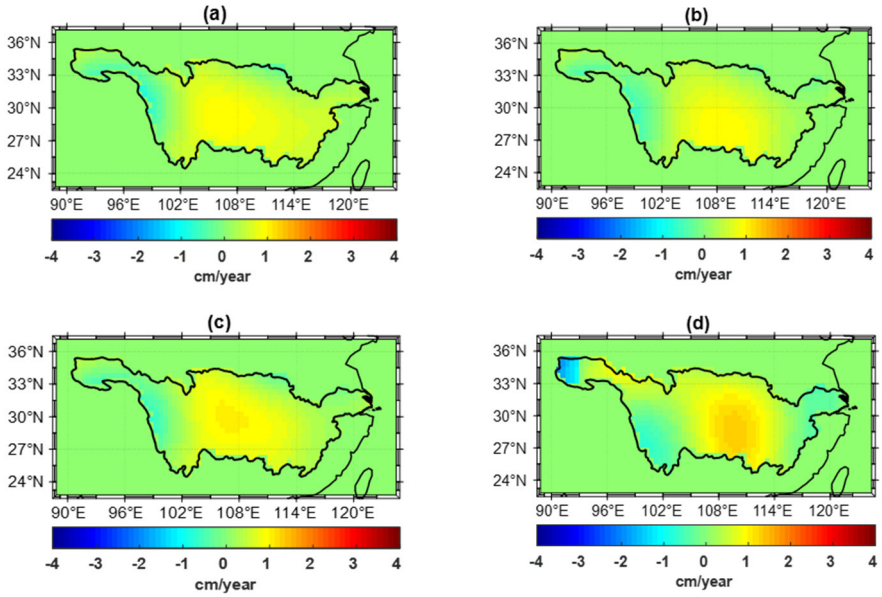

Fig. 13. Spatial distribution of secular trend of mascons. (a) P4M6 + 300 km Gaussian filtering. (b) Tikhonov regularization. (c) Adaptive regularization. (d) TSVD regularization.

algorithm [63], [64]. The time series in Fig. 14 consist well either in the time domain or frequency domain. Since the derived time series exhibits a significant linear trend and seasonal variations with semiannual and annual periods, we fit them with the following harmonic model:

$$\mathrm{EWH}(t) = a + b \cdot t + \sum_{k=1}^{2} \left(A_k \sin\left(\frac{2\pi}{T_k} t - \theta_k\right) + B_k \cos\left(\frac{2\pi}{T_k} t - \theta_k\right) \right) + \Delta \quad (55)$$

where a and b denote the constant and velocity, respectively, $A_k, B_k, \theta_k (k = 1, 2)$ stand for annual and semiannual amplitudes and phases, t is the time tag in a decimal year, $T_1 = 1$, $T_2 = 0.5$ are the periods in a year, and Δ is residual. Table II presents the fitting parameters of the time series

TABLE II
LINEAR TREND AND ANNUAL AND SEMIANNUAL SIGNALS OF THE TOTAL MASS VARIATION IN YANGTZE RIVER BASIN

Method	Trend (mm/year)	Amplitudes (cm)		RMSE (cm)
		Annual	Semi-annual	
Tikhonov	4.32	3.21	0.63	0.63
TSVD	4.08	3.21	0.69	0.64
Adaptive	4.41	3.33	0.95	0.56

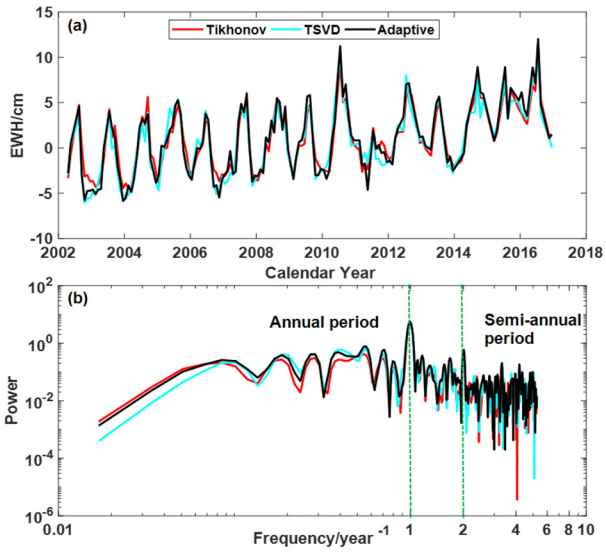

Fig. 14. Time series of mascon flux in Yangtze River in the time domain and frequency domain. (a) Time series of mascon flux. (b) Lomb-scrage periodical program.

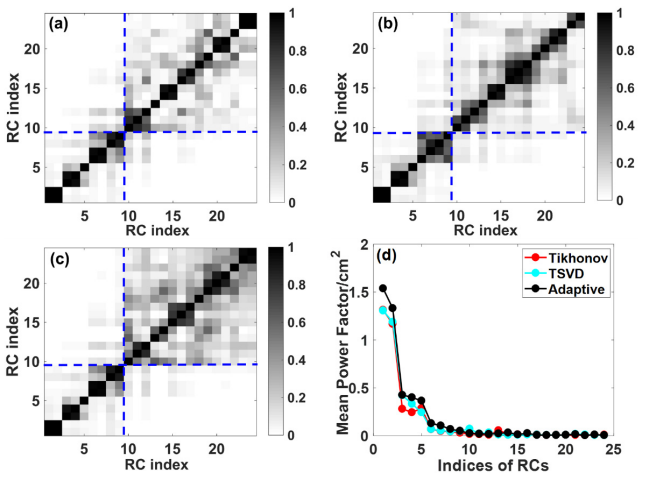

Fig. 15. w-correlations of the first leading 24 RCs and the mean powers. (a) Tikhonov. (b) TSVD. (c) Adaptive. (d) Mean power of extracted three signals.

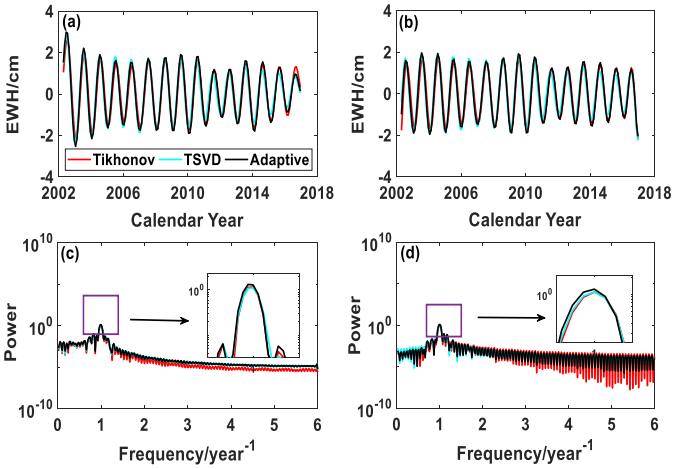

Fig. 16. RC pairs of annual signals and their spectrograms. (a) and (b) RC pairs. (c) and (d) Spectrograms.

with a nonlinear LS approach. It indicates that the mass of the Yangtze River Basin has generally increased during the period from April 2002 to December 2016, with a trend of 4.32 mm/year for the Tikhonov solution, 4.08 mm/year for the TSVD solution, and 4.41 mm/year for the adaptive solution. Furthermore, the amplitudes of periodic signals derived by the adaptive regularized solution are bigger than those by Tikhonov and TSVD regularized solutions. To evaluate the accuracy of the derived time series, we compute the root-mean-square error (RMSE) of each solution with the fit residuals and present them also in Table II, where the RMSE of our adaptive regularized solution is 0.56 cm, smaller than 0.63 cm in the case of Tikhonov solution and 0.64 cm in the case of TSVD solution. In other words, the improvements of our adaptive regularized solution relative to Tikhonov and TSVD regularized solutions in terms of RMSE are 11.11% and 12.50%, respectively.

Because of the complexity of the geophysical process, the seasonal oscillations in geodetic time series usually show a time-variable characteristic [65], [66]. The singular spectrum analysis (SSA) is a powerful, nonparametric, and data-driven time series decomposition tool. It has been proven to be successful in the identification of time-variable signals in noisy time series [67], [68], [69]. Since the derived mass variation series have missing values, we use improved SSA (ISSA) [70] to extract seasonal signals from incomplete time series. According to Golyandina [71], the window size had better be proportional to the period but not larger than half of the length of the series. We choose 24 months as the window size, which is two times the annual period. The weighted w-correlation method [71] is used to determine the reconstructed order. Fig. 15 presents the w-correlations and the mean power (variance) of 24 reconstructed components (RCs) for three regularizations. It is obvious that when $i, j > 9$, the w-correlations between ith RC and jth RC are really high, which means that these RCs cannot be well distinguished. Furthermore, we find that the first nine RCs can capture most of the signals, with a total percentage of 94.02% for Tikhonov, 93.71% for TSVD, and 95.02% for our adaptive method. The signal-to-noise ratios (SNRs) of the time series for ordinary Tikhonov, TSVD, and adaptive regularizations are 11.97, 11.73, and 12.80 dB, respectively. The results demonstrate that our adaptive regularization can extract more signals from the mass flux time series compared to the ordinary Tikhonov and TSVD regularizations. By performing spectrum analysis on each RC, we can obtain the periodic signals with the specific frequency we are interested in. In the grouping step of the SSA algorithm, the dominant reconstructed periodic signals tend to appear as a pair of components [71]. Figs. 16 and 17 present the component pairs of annual and semiannual signals and their spectrograms, from which we can find that the power of periodic signals derived by our adaptive regularization is significantly higher than those by the other two regularizations. Fig. 18 shows the annual, semiannual, and

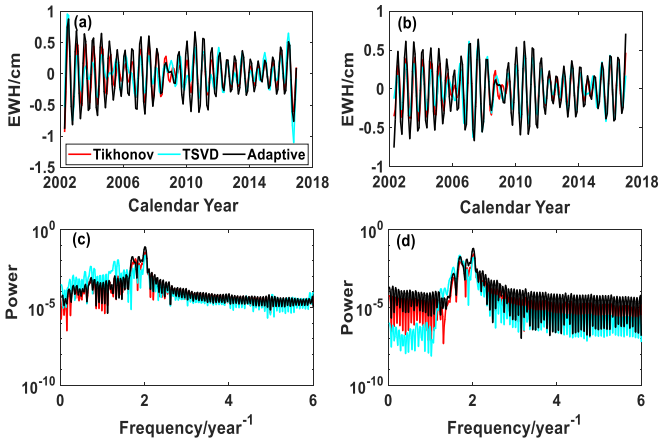

Fig. 17. RC pairs of semiannual signals and their spectrograms. (a) and (b) RC pairs. (c) and (d) Spectrograms.

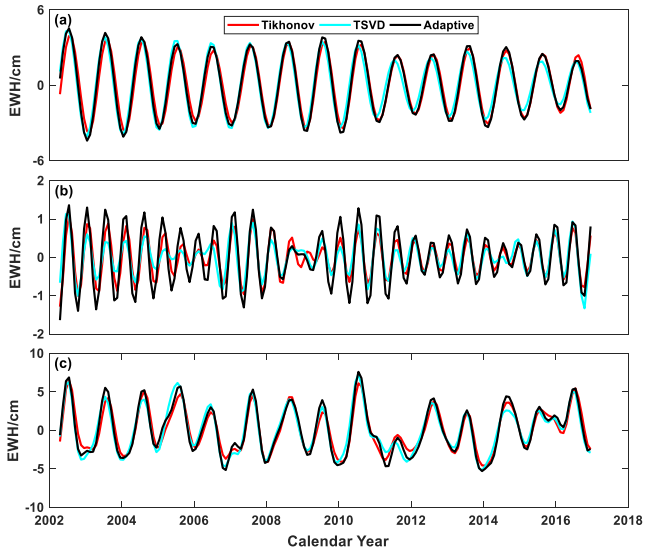

Fig. 18. Periodic signals extracted from mass variation series. (a) Annual signals. (b) Semiannual signals. (c) Total periodic signals.

TABLE III
MEAN POWER OF PERIODIC SIGNALS IN MASS VARIATION SERIES IN YANGTZE RIVER BASIN (cm^2)

	Periodic signals		
Method	Annual	Semi-annual	Total
Tikhonov	4.74	0.22	7.37
TSVD	4.85	0.19	8.22
Adaptive	5.55	0.46	9.54

total signals extracted from the mascon flux time series derived by three regularizations. It is clear that signals extracted by the three approaches consist well and show a significant time-variable amplitude. Table III presents the mean power of the derived signals, and the results show that our adaptive regularization can capture more signals, which further verifies the results given by a harmonic analysis and spectral analysis.

VI. CONCLUSION

In this article, an adaptive regularization has been developed to improve the accuracy of the solution to the ill-posed model.

Algorithm 1 Determining the Regularization Parameter

Input:
the index set S_2; the singular values $\lambda_i (i \in S_2)$; the vectors $\boldsymbol{v}_i (i \in S_2)$; the parameter estimate $\hat{\boldsymbol{x}}$ and the variance of unit weight σ_0^2; threshold δ
Output:
regularized parameter α
Begin
let $flag = 1$, $\alpha_0 = 0$;
select a positive number α_1;
while $flag = 1$ **then**
compute the value H with Eq.(A.3);
if $H < 0$ **then**
update $\alpha_1 \leftarrow 2\alpha_1$;
else
$flag = 0$;
end if
end while
set $flag = 1$;
while $flag = 1$ **then**
compute $\alpha_m = (\alpha_0 + \alpha_1)/2$;
compute the value H with Eq.(A.3);
if $abs(H) < \delta | abs(\alpha_1 - \alpha_0) < \delta$ **then**
$flag = 0$;
else if $H < 0$ **then**
update $\alpha_0 = \alpha_m$;
else
update $\alpha_1 = \alpha_m$;
end if
end while
End

The new method gives a more flexible regularized solution in spectral form, dividing the terms of different frequencies into three parts: 1) the terms of low frequency should not be regularized, i.e., keeping the characteristic of LS; 2) the terms of medium frequency should be regularized by the Tikhonov method; and 3) the terms of high-frequency should be regularized by the TSVD method, i.e., be truncated. The analytical conditions for determining the term sets are derived based on the criteria: the introduced bias should be smaller than the reduced errors; in other words, the MSE should be reduced. The proposed adaptive regularization is an advanced version of ordinary Tikhonov and TSVD regularization. Compared with the Tikhonov regularization, the new method can retain more signals in low-frequency and suppress noise in high-frequency more effectively. Compared with the TSVD method, the new method can more flexibly treat the medium-frequency terms.

Two examples have been presented to demonstrate the performance of our adaptive regularization. In the first numerical example, the repeated simulations reveal that our method can reduce the MSEs by about 25.00% and 9.09% relative to those of ordinary Tikhonov and TSVD methods, respectively. The second example is to retrieve the mass variation of Earth's surface with satellite gravity data based on the mascon model. The results clearly demonstrate that the mean MSEs of

Algorithm 2 Compute the Adaptive Regularized Solution

Input:
design matrix $\boldsymbol{A}$;
observation vector $\boldsymbol{y}$;
initial regularization parameter α_u;
threshold δ, maximum iteration number *maxiter*
Output:
the adaptive regularized solution $\hat{\boldsymbol{x}}_u$
Begin
decompose $\boldsymbol{A}$ as $\boldsymbol{A} = \sum_{i=1}^{n} \lambda_i \boldsymbol{u}_i \boldsymbol{v}_i^T$;
set $S_1 = \emptyset$, $S_2 = \mathbb{Z}$, cnt $= 1$;
compute the regularized solution $\hat{\boldsymbol{x}}_u$ with Eq.(14);
update the regularization parameter α_u with algorithm 1;
compute the variance of the unit weight $\hat{\sigma}_0^2$;
update the index sets of S_1 and S_2;
update $\hat{\boldsymbol{x}}_o \leftarrow \hat{\boldsymbol{x}}_u$;
compute the MSE of solutions mse_0;
let $\alpha_1 = \alpha_2 = \alpha_u$;
while true **do**
if cnt $>$ *maxiter* **then** break; **end if**
if $S_2 = \emptyset$, **then** $\alpha_u = 0$;
else
update the regularization parameter α_u;
end if
update the regularized solution $\hat{\boldsymbol{x}}_u$ with α_u;
update the variance of the unit weight $\hat{\sigma}_0^2$;
compute the MSE of solutions mse_1;
compute the difference $\Delta mse = mse_1 - mse_0$;
if $\Delta mse > 0 || abs(\Delta mse) < \delta$ **then**
if $\alpha_2 > \alpha_1$ **then**
update α_u within $(0, \alpha_1)$ with minimum MSE criteria;
update the index sets of S_1 and S_2
else break; **end if**
else
update the index sets of S_1 and S_2;
update $\hat{\boldsymbol{x}}_o \leftarrow \hat{\boldsymbol{x}}_u$;
update $\alpha_2 \leftarrow \alpha_u$;
update $mse_0 \leftarrow mse_1$
end if
cnt $=$ cnt $+ 1$;
end while
End

mascon parameters for 157 months derived by our method are 1.7155 cm, which is smaller than 1.9811 cm for the Tikhonov solution and 1.9428 cm for the TSVD solution. Furthermore, the spatial resolution of secular trend derived by our method is improved compared with the other two regularizations. The spectrum analysis and harmonic analysis show that there exist significant periodic (annual and semiannual) signals in derived time series of mass flux. The ISSA is employed to investigate the time-varying seasonal variation. The results show that the SNR of the extracted periodic signals from the adaptive regularized solution is stronger than those from the other two regularized solutions.

APPENDIX A

By comparing (20) and (21), it is clear that the regularization parameter α reduces the impact of observation error on the covariance of estimated parameters, especially for the high-frequency terms with small singular values, but it will introduce the biases to the estimated parameters. Therefore, minimizing the traced MSE is a reasonable criterion to determine the best regularization parameter. The traced $M(\hat{\boldsymbol{x}}_u)$ is

$$\mathrm{Tr}(M(\hat{\boldsymbol{x}}_u)) = \sum_{i\in S_1} \frac{\sigma_0^2}{\lambda_i^2} + \sum_{i\in S_2} \frac{\sigma_0^2\lambda_i^2 + \alpha^2\left(\boldsymbol{v}_i^T\bar{\boldsymbol{x}}\right)^2}{\left(\lambda_i^2+\alpha\right)^2} + \sum_{i\in S_3}\left(\boldsymbol{v}_i^T\bar{\boldsymbol{x}}\right)^2. \tag{A.1}$$

Taking the derivative of $\mathrm{Tr}(M(\hat{\boldsymbol{x}}_u))$ relative to α, we have

$$\frac{d}{d\alpha}\mathrm{Tr}(M(\hat{\boldsymbol{x}}_u)) = 2\sum_{i\in S_2} \frac{\lambda_i^2\left(\alpha\left(\boldsymbol{v}_i^T\bar{\boldsymbol{x}}\right)^2 - \sigma_0^2\right)}{\left(\lambda_i^2+\alpha\right)^3}. \tag{A.2}$$

By letting (A2) be zero, thus we obtain the algebraic equation

$$H(\alpha) = \sum_{i\in S_2} \frac{\lambda_i^2\left(\alpha\left(\boldsymbol{v}_i^T\bar{\boldsymbol{x}}\right)^2 - \sigma_0^2\right)}{\left(\lambda_i^2+\alpha\right)^3} = 0. \tag{A.3}$$

Since (A3) is a nonlinear equation of α, the bisection method is used to numerically solve the root of the equation [27]. Considering that the true values of parameters $\bar{\boldsymbol{x}}$ and the unit weight variance σ_0^2 are unknown, we replace them with the corresponding estimates. The specific algorithm flow is presented in Algorithm 1.

APPENDIX B

The flowchart of the algorithm for computing the adaptive regularized solution to ill-posed models is presented in Algorithm 2.

REFERENCES

[1] J. Hadamard, *Lectures on the Cauchy's Problem in Linear Partial Differential Equations*. New Haven, CT, USA: Yale Univ. Press, 1923.
[2] Y. Shen and B. Li, "Regularized solution to fast GPS ambiguity resolution," *J. Surveying Eng.*, vol. 133, no. 4, pp. 168–172, 2007.
[3] B. Li, Y. Shen, and Y. Feng, "Fast GNSS ambiguity resolution as an ill-posed problem," *J. Geodesy*, vol. 84, no. 11, pp. 683–698, Nov. 2010.
[4] B. Li, Y. Feng, Y. Shen, and C. Wang, "Geometry-specified troposphere decorrelation for subcentimeter real-time kinematic solutions over long baselines," *J. Geophys. Res.*, vol. 115, no. B11, p. B11404, 2010, doi: 10.1029/2010JB007549.
[5] D. B. Wen, Y. Wang, and R. Norman, "A new two-step algorithm for ionospheric tomography solution," *GPS Solutions*, vol. 16, no. 1, pp. 89–94, Jan./Feb. 2012.
[6] J. Tang and X. Gao, "Adaptive regularization method for 3-D GNSS ionospheric tomography based on the U-curve," *IEEE Trans. Geosci. Remote Sens.*, vol. 59, no. 6, pp. 4547–4560, Jun. 2021.
[7] C. Reigber *et al.*, "An Earth gravity field model complete to degree and order 150 from GRACE: EIGEN-GRACE02S," *J. Geodyn.*, vol. 39, no. 1, pp. 1–10, Jan. 2005.
[8] D. D. Rowlands *et al.*, "Global mass flux solutions from grace: A comparison of parameter estimation strategies—Mass concentrations versus Stokes coefficients," *J. Geophys. Res.*, vol. 115, no. B1, p. B01403, 2010, doi: 10.1029/2009JB006546.
[9] H. Save, S. Bettadpur, and B. D. Tapley, "High-resolution CSR GRACE RL05 mascons," *J. Geophys. Res., Solid Earth*, vol. 121, no. 10, pp. 7547–7569, 2016.

[10] F. Yang, J. Kusche, E. Forootan, and R. Rietbroek, "Passive-ocean radial basis function approach to improve temporal gravity recovery from GRACE observations," *J. Geophys. Res., Solid Earth*, vol. 122, no. 8, pp. 6875–6892, Aug. 2017.

[11] Q. Chen *et al.*, "An optimized short-arc approach: Methodology and application to develop refined time series of Tongji-Grace2018 GRACE monthly solutions," *J. Geophys. Res., Solid Earth*, vol. 124, no. 6, pp. 6010–6038, 2019.

[12] Q. Chen, Y. Shen, J. Kusche, W. Chen, T. Chen, and X. Zhang, "High-resolution GRACE monthly spherical harmonic solutions," *J. Geophys. Res., Solid Earth*, vol. 126, no. 1, 2020, Art. no. e2019JB018892.

[13] B. Zhong, J. Tan, Q. Li, X. Li, and T. Liu, "Simulation analysis of regional surface mass anomalies inversion based on different types of constraints," *Geodesy Geodyn.*, vol. 12, no. 4, pp. 298–307, Jul. 2021.

[14] J. Kusche and R. Klees, "Regularization of gravity field estimation from satellite gravity gradients," *J. Geodesy*, vol. 76, nos. 6–7, pp. 359–368, Jul. 2002.

[15] R. Pail *et al.*, "First GOCE gravity field models derived by three different approaches," *J. Geodesy*, vol. 85, no. 11, pp. 819–843, 2011.

[16] Y. Zhang, Y. Lu, L. Wang, and X. Huang, "A new approach on optimization of the rational function model of high-resolution satellite imagery," *IEEE Trans. Geosci. Remote Sens.*, vol. 50, no. 7, pp. 2758–2764, Jul. 2012.

[17] S. Gholinejad, A. Amiri-Simkooei, S. H. Alizadeh Moghaddam, and A. Alizadeh Naeini, "An automated PCA-based approach towards optimization of the rational function model," *ISPRS J. Photogramm. Remote Sens.*, vol. 165, pp. 133–139, Jul. 2020.

[18] S. Gholinejad, A. A. Naeini, and A. Amiri-Simkooei, "Optimization of RFM problem using linearly programed ℓ_1-regularization," *IEEE Trans. Geosci. Remote Sens.*, vol. 60, 2022, Art. no. 5601009.

[19] P. Li and Q. Wang, "Retrieval of leaf biochemical parameters using PROSPECT inversion: A new approach for alleviating ill-posed problems," *IEEE Trans. Geosci. Remote Sens.*, vol. 49, no. 7, pp. 2499–2506, Jul. 2011.

[20] X. Quan, B. He, and X. Li, "A Bayesian network-based method to alleviate the ill-posed inverse problem: A case study on leaf area index and canopy water content retrieval," *IEEE Trans. Geosci. Remote Sens.*, vol. 53, no. 12, pp. 6507–6517, Dec. 2015.

[21] H. Yu, M. Xing, and Z. Bao, "A fast phase unwrapping method for large-scale interferograms," *IEEE Trans. Geosci. Remote Sens.*, vol. 51, no. 7, pp. 4240–4248, Jul. 2013.

[22] H. Yu, Y. Lan, J. Xu, D. An, and H. Lee, "Large-scale L^0-norm and L^1-norm 2-D phase unwrapping," *IEEE Trans. Geosci. Remote Sens.*, vol. 55, no. 8, pp. 4712–4728, Aug. 2017.

[23] A. N. Tikhonov, "Regularization of ill-posed problems," *Doklady Akademii Nauk SSSR*, vol. 151, no. 1, pp. 49–52, 1963.

[24] A. N. Tikhonov, "Solution of incorrectly formulated problems and the regularization method," *Doklady Akademii Nauk SSSR*, vol. 151, no. 3, pp. 501–504, 1963.

[25] A. E. Hoerl and R. W. Kennard, "Ridge regression: Applications to nonorthogonal problems," *Technometrics*, vol. 12, no. 1, pp. 69–82, 1970.

[26] A. E. Hoerl and R. W. Kennard, "Ridge regression: Biased estimation for nonorthogonal problems," *Technometrics*, vol. 12, no. 1, pp. 55–67, 1970.

[27] P. Xu, "Determination of surface gravity anomalies using gradiometric observables," *Geophys. J. Int.*, vol. 110, no. 2, pp. 321–332, Aug. 1992.

[28] P. Xu and R. Rummel, "A simulation study of smoothness methods in recovery of regional gravity fields," *Geophys. J. Int.*, vol. 117, no. 2, pp. 472–486, 1994.

[29] G. H. Golub, M. Heath, and G. Wahba, "Generalized cross-validation as a method for choosing a good ridge parameter," *Technometrics*, vol. 21, no. 2, pp. 215–223, May 1979.

[30] P. C. Hansen and D. P. O'leary, "The use of the L-curve in the regularization of discrete Ill-posed problems," *SIAM J. Sci. Comput.*, vol. 14, no. 6, pp. 1487–1503, Jul. 1993.

[31] K.-R. Koch and J. Kusche, "Regularization of geopotential determination from satellite data by variance components," *J. Geodesy*, vol. 76, no. 5, pp. 259–268, May 2002.

[32] P. C. Hansen, "The truncated SVD as a method for regularization," *BIT*, vol. 27, pp. 543–553, Dec. 1987.

[33] P. Xu, "Truncated SVD methods for discrete linear ill-posed problems," *Geophys. J. Int.*, vol. 135, no. 2, pp. 505–514, 1998.

[34] K. Liu, "Using liu-type estimator to combat collinearity," *Commun. Statist.-Theory Methods*, vol. 32, no. 5, pp. 1009–1020, Jan. 2003.

[35] K. Liu, "More on Liu-type estimator in linear regression," *Commun. Statist.-Theory Methods*, vol. 33, no. 11, pp. 2723–2733, 2004.

[36] T. J. Ulrych, M. D. Sacchi, and A. Woodbury, "A Bayes tour of inversion: A tutorial," *Geophysics*, vol. 66, no. 1, pp. 55–69, 2001.

[37] P. Xu, "A new look at Akaike's Bayesian information criterion for inverse ill-posed problems," *J. Franklin Inst.*, vol. 358, no. 7, pp. 4077–4102, 2021.

[38] D. Chen, B. Hofmann, and J. Zou, "Elastic-net regularization versus ℓ_1-regularization for linear inverse problems with quasi-sparse solutions," *Inverse Problems*, vol. 33, no. 1, 2016, Art. no. 015004.

[39] A. Tarantola, *Inverse Problem Theory and Methods for Model Parameter Estimation*. Philadelphia, PA, USA: SIAM, 2005, pp. 81–96.

[40] A. N. Tikhonov and V. Y. Arsenin, *Solutions of Ill-Posed Problems*. New York, NY, USA: Wiley, 1977.

[41] V. A. Morozov, *Methods for Solving Incorrectly Posed Problems*. Berlin, Germany: Springer, 1984, doi: 10.1007/978-1-4612-5280-1.

[42] A. N. Tikhonov, A. V. Goncharsky, V. V. Stepanov, and A. G. Yagola, "Numerical methods for the approximate solution of ill-posed problems on compact sets," in *Numerical Methods for the Solution of Ill-Posed Problems*. Dordrecht, The Netherlands: Springer, 1995, pp. 65–79.

[43] P. C. Hansen, "Regularization tools version 4.1 for MATLAB 7.3," *Numer. Algorithms*, vol. 46, pp. 189–194, Mar. 2007.

[44] P. Xu, Y. Shen, Y. Fukuda, and Y. Liu, "Variance component estimation in linear inverse ill-posed models," *J. Geodesy*, vol. 80, no. 2, pp. 69–81, 2006.

[45] P. Xu, "Iterative generalized cross-validation for fusing heteroscedastic data of inverse ill-posed problems," *Geophys. J. Int.*, vol. 179, no. 1, pp. 182–200, 2009.

[46] B. Li, M. Wang, and Y. Shen, "The hypothesis testing statistics in linear ill-posed models," *J. Geodesy*, vol. 95, no. 1, Jan. 2021.

[47] Y. Shen, P. Xu, and B. Li, "Bias-corrected regularized solution to inverse ill-posed models," *J. Geodesy*, vol. 86, no. 8, pp. 597–608, 2012.

[48] T. Chen, J. Kusche, Y. Shen, and Q. Chen, "A combined use of TSVD and Tikhonov regularization for mass flux solution in Tibetan plateau," *Remote Sens.*, vol. 12, no. 12, p. 2045, Jun. 2020.

[49] P. Meincke, "Linear GPR inversion for lossy soil and a planar air-soil interface," *IEEE Trans. Geosci. Remote Sens.*, vol. 39, no. 12, pp. 2713–2721, Dec. 2001.

[50] J. Guo and R. Xie, "An inversion of NMR echo data based on a normalized iterative hard thresholding algorithm," *IEEE Geosci. Remote Sens. Lett.*, vol. 15, no. 9, pp. 1332–1336, Sep. 2018.

[51] R. Lang and H. Saleh, "Microwave inversion of leaf area and inclination angle distributions from backscattered data," *IEEE Trans. Geosci. Remote Sens.*, vol. GE-23, no. 5, pp. 685–694, Sep. 1985.

[52] B. Liu, X. Zou, S. Yi, N. Sneeuw, J. Cai, and J. Li, "Identifying and separating climate- and human-driven water storage anomalies using GRACE satellite data," *Remote Sens. Environ.*, vol. 263, Sep. 2021, Art. no. 112559.

[53] S. Gao *et al.*, "Spatiotemporal variability of global river extent and the natural driving factors revealed by decades of landsat observations, GRACE gravimetry observations, and land surface model simulations," *Remote Sens. Environ.*, vol. 267, Dec. 2021, Art. no. 112725.

[54] P. Castellazzi, R. Chopping, and C. Brouard, "Mining exports and climate variability influencing grace-derived water storage trend estimates in Australia," in *Proc. IEEE Int. Geosci. Remote Sens. Symp. (IGARSS)*, Waikoloa, HI, USA, Sep. 2020, pp. 5069–5072.

[55] X. Li, B. Zhong, J. Li, and R. Liu, "Analysis of terrestrial water storage changes in the Shaan-Gan-Ning Region using GPS and GRACE/GFO," *Geodesy Geodyn.*, vol. 13, no. 2, pp. 179–188, 2022.

[56] M. K. Cheng, J. C. Ries, and B. D. Tapley, "Geocenter variations from analysis of SLR data," in *Reference Frames for Applications in Geosciences*. Berlin, Germany: Springer, 2013, pp. 19–25.

[57] B. D. Loomis, K. E. Rachlin, and S. B. Luthcke, "Improved Earth oblateness rate reveals increased ice sheet losses and mass-driven sea level rise," *Geophys. Res. Lett.*, vol. 46, no. 12, pp. 6910–6917, 2019.

[58] B. D. Loomis, K. E. Rachlin, D. N. Wiese, F. W. Landerer, and S. B. Luthcke, "Replacing GRACE/GRACE-FO with satellite laser ranging: Impacts on Antarctic Ice Sheet mass change," *Geophys. Res. Lett.*, vol. 47, no. 3, 2020, Art. no. e2019GL085488.

[59] W. Richard Peltier *et al.*, "Comment on 'an assessment of the ICE-6G_C (VM5a) glacial isostatic adjustment model' by Purcell et al.," *J. Geophys. Res., Solid Earth*, vol. 123, no. 2, pp. 2019–2028, 2018.

[60] L. Wang, C. Chen, X. Ma, Z. Fu, Y. Zheng, and Z. Peng, "Evaluation of GRACE mascon solutions using *in-situ* geodetic data: The case of hydrologic-induced crust displacement in the Yangtze river basin," *Sci. Total Environ.*, vol. 707, Mar. 2020, Art. no. 135606.

[61] S. Yang, W. Zheng, W. Yin, and J. Liu, "Improve the accuracy of GRACE terrestrial water storage changes using GRACE data combined with a new scale factor correction method," *Chin. J. Geophys.*, vol. 64, no. 9, pp. 3068–3082, 2021.

[62] L. Wang, M. K. Kaban, M. Thomas, C. Chen, and X. Ma, "The challenge of spatial resolutions for GRACE-based estimates volume changes of larger man-made lake: The case of China's Three Gorges Reservoir in the Yangtze River," *Remote Sens.*, vol. 11, no. 1, p. 99, 2019.

[63] J. D. Scargle, "Studies in astronomical time series analysis. II–Statistical aspects of spectral analysis of unevenly spaced data," *Astrophys. J.*, vol. 263, p. 835, Dec. 1982.

[64] W. H. Press, S. A. Teukolsky, W. T. Vettering, and B. P. Flannery, "Numerical recipes in C++: The art of scientific computing (2nd EDN) 1 numerical recipes example book (C++) (2nd EDN) 2 numerical recipes multi-language code CD ROM with LINUX or UNIX single-screen license revised version 3," *Eur. J. Phys.*, vol. 24, no. 3, pp. 329–330, May 2003.

[65] A. Klos, M. S. Bos, and J. Bogusz, "Detecting time-varying seasonal signal in GPS position time series with different noise levels," *GPS Solutions*, vol. 22, no. 1, p. 21, 2018.

[66] K. Ji, Y. Shen, and F. Wang, "Signal extraction from GNSS position time series using weighted wavelet analysis," *Remote Sens.*, vol. 12, no. 6, p. 992, Mar. 2020.

[67] N. Golyandina, A. Korobeynikov, and A. Zhigljavsky, *Singular Spectrum Analysis for Time Series*. Berlin, Germany: Springer, 2018, pp. 1–272, doi: 10.1007/978-3-662-57380-8.

[68] F. Wang, Y. Shen, T. Chen, Q. Chen, and W. Li, "Improved multichannel singular spectrum analysis for post-processing GRACE monthly gravity field models," *Geophys. J. Int.*, vol. 223, no. 2, pp. 825–839, 2020.

[69] Y. Shen, F. Wang, and Q. Chen, "Weighted multichannel singular spectrum analysis for post-processing GRACE monthly gravity field models by considering the formal errors," *Geophys. J. Int.*, vol. 226, no. 3, pp. 1997–2010, Jun. 2021.

[70] Y. Shen, F. Peng, and B. Li, "Improved singular spectrum analysis for time series with missing data," *Nonlinear Processes Geophys.*, vol. 22, no. 4, pp. 371–376, Jul. 2015.

[71] N. Golyandina, "On the choice of parameters in singular spectrum analysis and related subspace-based methods," *Statist. Its Interface*, vol. 3, no. 3, pp. 259–279, 2010.

Kunpu Ji received the B.S. degree in surveying engineering from the School of Geomatics Science and Technology, Nanjing Tech University, Nanjing, China, in 2017, and the M.S. degree in geodesy from the College of Surveying and Geo-Informatics, Tongji University, Shanghai, China, in 2020, where he is currently pursuing the Ph.D. degree.

His main research interests include geodetic inversion problems and geodetic time series analysis.

Yunzhong Shen received the Ph.D. degree in geophysical geodesy from the Institute of Geodesy and Geophysics, Chinese Academy of Sciences, Beijing, China, in 2000.

He is currently a Professor with the College of Surveying and Geo-informatics, Tongji University, Shanghai, China. His research interests include geodetic data processing on satellite positioning and satellite gravimetry. His main research works include the regularized solution to the ill-conditioned inverse problem on recovering a gravitational potential model from satellite-to-satellite tracking data, and variance component and parameter estimation theory in mixed-integer models of multisystem and triple-frequency global navigation satellite system (GNSS) observations.

Dr. Shen is an Editor of *Journal of Geodesy* and *Acta Geodetica et Cartographica Sinica*.

Qiujie Chen received the B.S. degree in surveying and mapping engineering from the Guangdong University of Technology, Guangzhou, Guangdong, China, in 2007, and the Ph.D. degree in geodesy from Tongji University, Shanghai, China, in 2016.

He is currently a Professor with the College of Surveying and Geo-Informatics, Tongji University. His research interests include short-arc approach for satellite-based gravity field determination, frequency-dependent noise modeling, non-gravitational acceleration calibration, regularization methodologies, mascon modeling, and simulations for next-generation gravity satellites.

Bofeng Li received the B.S. and Ph.D. degrees in geodesy from Tongji University, Shanghai, China, in 2005 and 2010, respectively.

He is currently a Professor with the College of Surveying and Geo-informatics, Tongji University. His research interests include global navigation satellite system (GNSS) ambiguity resolution, precise orbit determination, real-time precise positioning, and multisensor integrated seamless positioning.

Wei Wang received the B.S. degree in surveying and geoinformatics from the Shandong University of Science and Technology, Qingdao, China, in 2019. She is currently pursuing the Ph.D. degree with the College of Surveying and Geo-Informatics, Tongji University, Shanghai, China.

Her research interests include mascon modeling from time-variable gravity model and its application on hydrology and cryosphere.